Decoration of ZnO nanocrystals on the surface of shuttle-shaped Mn_2O_3 and its magnetic-optical properties†

Yong Hu,*[a] Haisheng Qian,[a] Changfa Guo[a] and Ting Mei*[b]

Received 25th November 2009, Accepted 28th April 2010
DOI: 10.1039/b924820j

A new type of magnetic-fluorescent bifunctional nanocomposites, shuttle-shaped Mn_2O_3 decorated by ZnO nanocrystals has been successfully prepared by a facile two-step, wet-chemical strategy.

Introduction

During the past few years, various morphologies of oxide nanostructures, such as nanobelts, nanowires, nanotubes, nanocombs, and nanorings *etc*., have been successfully synthesized.[1–3] Despite the fact that fabrication of simple oxide nanostructures has progressed significantly, preparation of multifunctional oxide nanostructures remains a challenge. Neither the fundamental growth behaviors nor the properties are well understood. Because nanocomposites are made from different materials, it may be necessary to combine the different physical properties into one nanostructure.[4] Thus fabrication of complex functional nanostructures is a crucial key towards the realization of functional nanodevices.[5–7] In particular, composite materials with magnetic and optical properties are of great importance in the fields of chemistry, biology, and medical sciences as well as in biotechnology.[8–11]

Compared to other wide band gap materials, zinc oxide (ZnO) has a large direct band gap of 3.37 eV, and a large exciton binding energy of 60 meV, which results in efficient excitonic emission at room temperature. ZnO is also a versatile material that has achievable applications in photocatalysts, varistors, sensors, piezoelectric transducers, solar cells, transparent electrodes, electroluminescent devices and ultraviolet (UV) laser diodes.[12–16] In particular, ZnO nanocrystals have superior optical properties in comparison to the bulk crystals due to the three-dimensional confinement of the carrier and phonon leads not only to continuous tuning of the optoelectronic properties but also leads to an improvement in the device performance.[17]

Manganese oxides with their outstanding structural flexibility combined with their novel chemical and physical properties, are of increasing importance due to their remarkable technical applications in catalysis for completely oxidizing various volatile organic substances or hydrocarbons, selective reduction of nitrobenzene and electrode materials.[18,19] Until now, manganese oxides were synthesized through a variety of methods, such as hydrothermal, arc evaporation, hydrothermal reduction, chemical liquid homogeneous precipitation and thermal decomposition, *etc*.[20–23]

Herein, we demonstrate a facile two-step, wet-chemical strategy for the decoration of ZnO nanocrystals on the surface of shuttle-shaped Mn_2O_3 nanocomposite. Firstly, high-quality ZnO nanocrystals were synthesized from zinc acetate dehydrate ($Zn(CH_3COO)_2 \cdot 2H_2O$) in diethylene glycol (DEG) at 160 °C for 1 h.[24] Secondly, shuttle-shaped Mn_2O_3 decorated by ZnO nanocrystals was obtained by refluxing $Mn(CH_3COO)_2 \cdot 4H_2O$, DEG in the above ZnO nanocrystals suspension at 100 °C for 3 h and polyvinylpyrrolidone (PVP) as a structure-directing agent. To the best of our knowledge, this shuttle morphology Mn_2O_3 has not been reported until now. The measurements of the optical and magnetic properties revealed that the as-prepared nanocomposites are bifunctional and have integrated the photoluminescent effect of ZnO nanocrystals and the magnetism of shuttle-shaped Mn_2O_3.

Experimental

All the chemical reagents were purchased from Sigma-Aldrich and used without further purification and distilled water was used throughout. Shuttle-shaped Mn_2O_3 decorated by ZnO nanocrystals nanocomposite were prepared in a two-step procedure.

Firstly, in a typical reaction, 2.19 g of $Zn(CH_3COO)_2 \cdot 2H_2O$ was introduced to a round bottom flask and dissolved in 100 mL of DEG. Then, the temperature of the reaction solution was increased to 160 °C and maintained for 1 h. The product was placed in a centrifuge with operating 6000 rpm for 30 min. After this procedure, the solution was separated into two gradations. The white bottom layer contained the secondary ZnO clusters and the transparent upper suspension included the dispersive single-crystalline ZnO nanocrystals. Unlike the secondary clusters, the single-crystalline ZnO nanocrystals were almost monodispersed because of the stable surface during the chemical reaction.[24]

Secondly, 1.2 g of $Mn(CH_3COO)_2 \cdot 4H_2O$ and 0.5 g of PVP were introduced to a round bottom three-neck flask and dissolved in 50 mL of DEG. When the temperature of the mixed solution was 80 °C, 20 mL of the above transparent upper ZnO nanocrystal suspension was added and stirring continued. Then the temperature of reaction solution was increased to 100 °C and aged for 3 h. Finally, the products were collected by centrifugation (6000 rpm/30 min), washed with ethanol and distilled water several times, and then dried in vacuum at 60 °C for 4 h.

Powder X-ray diffraction (XRD) measurement of the sample was performed with a Siemens D5005 X-ray diffractometer using Cu-Kα radiation at a scanning rate of 0.06° s^{-1}. Scanning electron microscopy (SEM) and energy-dispersive X-ray (EDS) measurements were performed with a Hitachi S-5200 scanning electron microanalyzer with an accelerating voltage 15 kV, after dispersing samples in

[a]*Zhejiang Key Laboratory for Reactive Chemistry on Solid Surfaces and Institute of Physical Chemistry, Zhejiang Normal University, Jinhua, 321004, P.R.China. E-mail: yonghu@zjnu.edu.cn; Fax: +86-579-82282595; Tel: +86-579-82282234*
[b]*School of Electrical and Electronic Engineering, Nanyang Technological University, Singapore 639798. E-mail: etmei@ntu.edu.sg*
† Electronic supplementary information (ESI) available: UV-vis spectrum of shuttle-shaped Mn_2O_3/ZnO nanocomposites and the Mn_2O_3 growth mechanism. See DOI: 10.1039/b924820j

ethanol and depositing on copper disk. Transmission electron microscopy (TEM) was conducted at 200 kV with a JEM-2100F field emission machine. Samples were prepared for TEM by dispersing the products in ethanol and placing several drops of the suspension on holey carbon films supported by copper grids. The PL spectra were measured at room temperature with a Fluorolog-3 spectrofluorimeter using an excitation wavelength of 325 nm. DC magnetization measurements were carried out in a Quantum Designed Physical Properties Measurement Systems (PPMS) instrument from 5 K to 300 K with an applied field of 100 O_e in zero-field-cooling (ZFC) and in-field-cooling (FC) modes.

Results and discussion

Fig. 1 shows the XRD pattern of as-prepared shuttle-shaped Mn_2O_3/ZnO nanocomposites. All of the peaks of the product can be indexed to body-centered cubic structured Mn_2O_3 (JCPDS card No. 89-4836) with cell parameters $a = 9.406$ Å. Due to the detection limit of about 2 wt%, we could not observe the ZnO characteristic peak.

A general overview SEM image in Fig. 2(a) shows that the product is completely composed of a shuttle-shaped structure 5–10 μm in length and 0.5–1 μm in central diameter. The high-magnification image (Fig. 2(b)) presents a perfect shuttle with some resembling particles on the surface. The side of the shuttle is shown in Fig. 2(c) and we can clearly calculate that the thickness of the shuttle is about 200 nm. Fig. 2(d) displays the associated EDS spectrum of shuttle-shaped Mn_2O_3 decorated by ZnO nanocrystal nanocomposites, which reveals the existence of ZnO nanocrystals on the Mn_2O_3 surface.

Further morphology characterization of the shuttle-shaped sample was performed on TEM, as shown in Fig. 3(a), which was in good agreement with the results of SEM. The composite material of ZnO nanocrystals decorating on the surface of shuttle-shaped Mn_2O_3 was clearly revealed in Fig. 3(b) and a representative HRTEM image with fast Fourier transform (FFT, inset in Fig. 3(b)) of ZnO nanocrystal (4–5 nm). It invariably revealed regular lattice spacings, and favorable cases, where the nanocrystal was aligned along a principal axis [10$\bar{1}$1] direction. The Fourier reconstruction yielded patterns consistent with ZnO wurzite structure.[25]

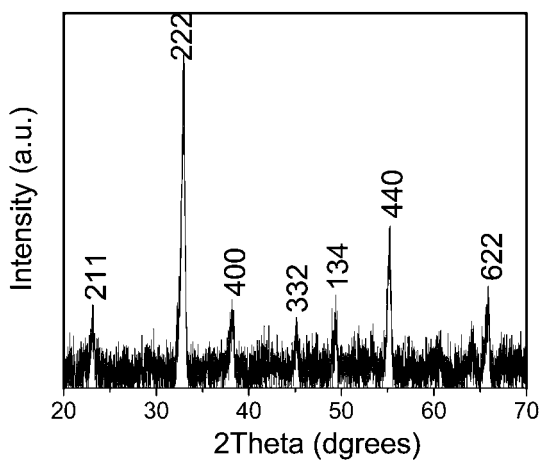

Fig. 1 XRD pattern of the as-prepared shuttle-shaped Mn_2O_3/ZnO nanocomposites.

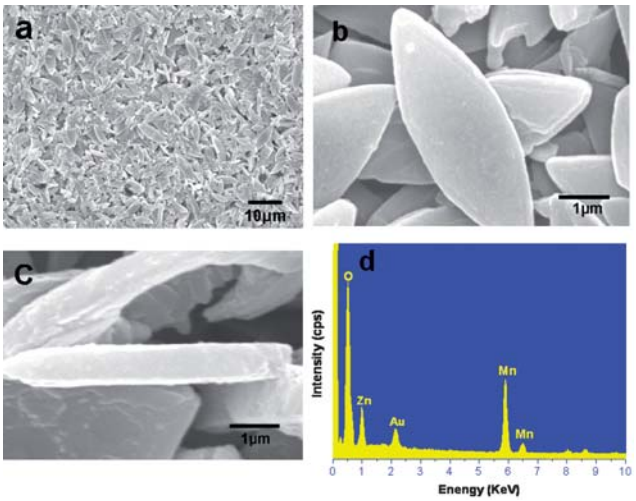

Fig. 2 SEM images of shuttle-shaped Mn_2O_3/ZnO nanocomposites refluxing in DEG at 100 °C for 3 h: (a) the image overview, (b) at high magnification, (c) the profile of the as-prepared product ~200 nm in thickness, and (d) EDS pattern of the as-prepared Mn_2O_3/ZnO nanocomposites.

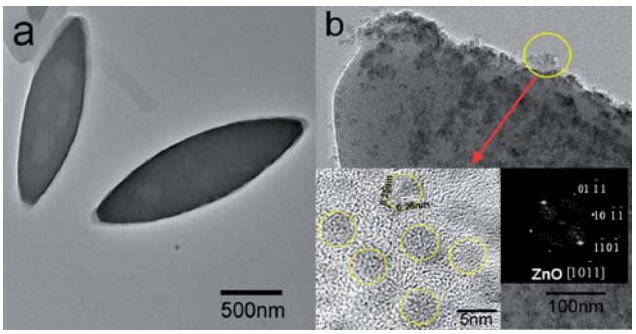

Fig. 3 TEM images of shuttle-shaped Mn_2O_3/ZnO nanocomposites: (a) at low magnification, (b) at high magnification and HRTEM image with FFT of ZnO nanocrystals (inset).

To gain a better understanding on the growth mechanism of shuttle-shaped Mn_2O_3/ZnO nanocomposites, the products formed without the structure-directing agent of PVP or ZnO nanocrystals were collected for SEM analysis, while other experimental conditions were kept the same (the Mn_2O_3 growth mechanism, see ESI†). From Fig. 4, only Mn_2O_3/ZnO platelets several micrometers in diameter were formed in the absence of PVP. Thus, the effect of the structure-directing agent, PVP, is evident and necessary. In addition, ZnO nanocrystals also have an important influence on the growth of shuttle-shaped Mn_2O_3, as we only observed sheet-like nanostructures of Mn_2O_3 formed after refluxing at 190 °C without the existence of ZnO nanocrystals.[26]

The optical properties of ZnO nanocrystals on the surface of shuttle-shaped Mn_2O_3 nanocomposites were characterized by UV-visible absorption (see ESI†) and PL spectroscopy, respectively. The PL spectrum was measured at room temperature, as shown in Fig. 5. A strong UV light emission peak is clearly observed at 367 nm, corresponding to a transition energy of 3.38 eV. A remarkable blue-shift of 0.12 eV with respect to the edge emission gap energy (3.26 eV)

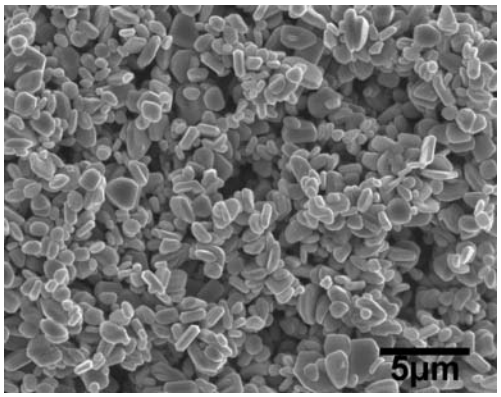

Fig. 4 SEM images of as-prepared Mn_2O_3/ZnO nanocomposites without the structure-directing agent, PVP.

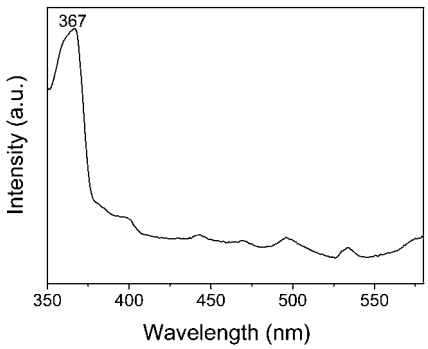

Fig. 5 The PL spectrum of shuttle-shaped Mn_2O_3/ZnO nanocomposites.

of bulk ZnO crystals is obtained due to the quantum confinement effect in the ZnO nanocrystals.[27]

The temperature dependence of field-cooled (FC) and zero-field-cooled (ZFC) magnetizations of shuttle-shaped Mn_2O_3 decorated by ZnO nanocrystals, measured on warming from 5 K to 300 K presents several magnetic features (Fig. 6). The high-temperature (>81 K) regions of the FC and ZFC magnetizations coincide and increase slowly with decreasing temperature. The susceptibility can be well described as paramagnetic by the Curie–Weiss law, $\chi = C/(T - \theta)$ (see inset in Fig. 6), with an effective magnetic moment, calculated by $\mu_{eff} = \sqrt{8C}\mu_B$ in the range of 0.58 μ_B. A downturn in magnetization

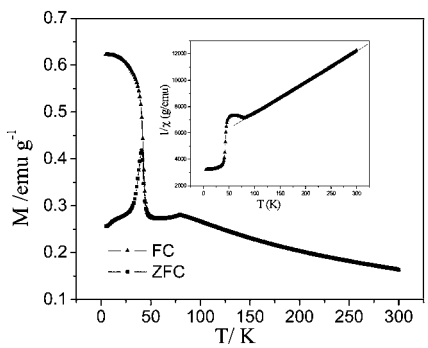

Fig. 6 *M vs. T* curve of shuttle-shaped Mn_2O_3/ZnO nanocomposites: temperature dependence of the inverse FC susceptibility (inset) and the red line is the fitting curve with Curie–Weiss law.

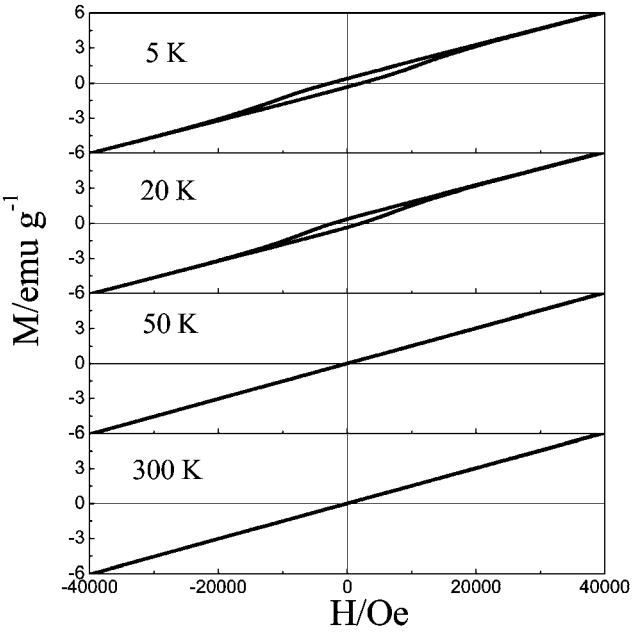

Fig. 7 *M vs. H* curve of shuttle-shaped Mn_2O_3/ZnO nanocomposites at different temperatures.

with onset at 81 K is consistent with antiferromagnetism, and coincides with observations from bulk Mn_2O_3 which orders antiferromagnetically from 80 to 100 K.[28–30] Below 41 K Mn_2O_3 shows an abrupt ferromagnetic rise in the magnetization, and a distinct divergence of the FC and ZFC magnetizations as reported for mesoporous Mn_2O_3.[31] The magnetization continues to increase with decreasing temperature in the FC curve, but decreases in the ZFC curve, presenting a spin-glass/cluster-glass behavior. Therefore, the magnetic properties of shuttle-shaped Mn_2O_3 progress from paramagnetism, to antiferromagnetism, ferromagnetism and finally a spin-glass/cluster-glass state, as the temperature is reduced from 300 K to 5 K.

These transitions of the magnetic properties for Mn_2O_3 are confirmed by the magnetic hysteresis loops (Fig. 7). At 300 K and 50 K the magnetism increases linearly without hysteresis, in a manner consistent with paramagnetic and antiferromagnetic properties. In the magnetic glassy state at 20 K and 5 K there is clear hysteresis with coercive fields of 2279 and 2565 Oe, and remanence of 0.365 and 0.385 emu g^{-1}, respectively, consistent with ferromagnetic clusters. However the magnetic curve does not reach saturation in external fields up to 4 T, suggesting antiferromagnetic clusters are present. Therefore, poor order correlation of the ferromagnetic and antiferromagnetic clusters at low temperatures creates a glassy state.

Conclusion

In summary, a new type of nanostructured composite, shuttle-shaped Mn_2O_3 decorated by ZnO nanocrystals has been successfully prepared by refluxing $Mn(CH_3COO)_2 \cdot 4H_2O$, DEG and the ZnO nanocrystals suspension at 100 °C for 3 h, in which PVP acts as a structure-directing agent. To the best of our knowledge, this shuttle-shaped morphology nanocomposite has not been achieved so far. The measurements of the properties demonstrated that the as-prepared nanocomposites are bifunctional, and have an integrated PL effect of ZnO nanocrystals and the magnetism of shuttle-shaped Mn_2O_3. These new structure nanocomposites may be promising

materials when applied in the fabrication of nanoscale magneto-optic devices. The synthesis method used in this work is simple and does not involve costly surfactants or sophisticated equipment; it provides a convenient route to synthesize bifunctional complex materials for advanced applications.

Acknowledgements

This material was based on research supported by the Scientific Research Foundation for the Returned Overseas Chinese Scholars, State Education Ministry, the Educational Commission of Zhejiang Province of China (Z200909406), the Singapore National Research Foundation under CRP Award (NRF-G-CRP 2007-01), and the National Natural Science Foundation of China (20806075).

Notes and references

1 X. Y. Kong, Y. Ding, R. Yang and Z. L. Wang, *Science*, 2004, **303**, 1348.
2 Y. N. Xia, P. D. Yang, Y. G. Sun, Y. Y. Wu, B. Mayers, B. Gates, Y. Yin, D. F. Kim and Y. Q. Yan, *Adv. Mater.*, 2003, **15**, 353.
3 J. X. Wang, X. W. Sun, S. S. Xie, Y. Yang, H. Y. Chen, G. Q. Lo and D. L. Kwong, *J. Phys. Chem. C*, 2007, **111**, 7671.
4 R. R. He, M. Law, R. Fan, F. Kim and P. D. Yang, *Nano Lett.*, 2002, **21**, 109.
5 M. S. Gudiksen, L. J. Lauhon, J. Wang, D. C. Smith and C. M. Lieber, *Nature*, 2002, **415**, 617.
6 C. D. Keating and M. J. Natan, *Adv. Mater.*, 2003, **15**, 451.
7 W. I. Park, G. C. Yi, M. Kim and S. J. Pennycook, *Adv. Mater.*, 2003, **15**, 526.
8 B. K. Oh, S. Park, J. E. Millstone, S. W. Lee, K. B. Lee and C. A. Mirkin, *J. Am. Chem. Soc.*, 2006, **128**, 11825.
9 K. Gunnarsson, P. E. Roy, S. Felton, J. Pihl, P. Svedlindh, S. Berner, H. Lidbaum and S. Oscarsson, *Adv. Mater.*, 2005, **17**, 1730.
10 V. L. Colvin, M. C. Schlamp and A. P. Alivisatos, *Nature*, 1994, **370**, 354.
11 Y. X. Zhang, G. K. Das, R. Xu and T. T. Y. Tan, *J. Mater. Chem.*, 2009, **19**, 3639.
12 F. C. Lin, Y. Takao, Y. Shimizu and M. Egashira, *Sens. Actuators, B*, 1995, **25**, 843.
13 J. B. Baxter and E. S. Aydil, *Appl. Phys. Lett.*, 2005, **86**, 053114.
14 R. L. Hoffman, B. J. Norris and J. F. Wager, *Appl. Phys. Lett.*, 2003, **82**, 733.
15 W. I. Park and G. C. Yi, *Adv. Mater.*, 2003, **16**, 1907.
16 T. Makino, C. Chia, Y. Segawa, M. Kawasaki, A. Ohtomo, K. Tamura, Y. Matsumoto and H. Koinuma, *Appl. Surf. Sci.*, 2002, **189**, 277.
17 H. M. Cheng, K. F. Lin, H. C. Hsu and W. F. Hsieh, *Appl. Phys. Lett.*, 2006, **88**, 261909.
18 Y. Chen, Y. Zhang, Q. Z. Yao, G. T. Zhou, S. Fu and H. Fan, *J. Solid State Chem.*, 2007, **180**, 1218.
19 K. Ramesh, L. Chen, F. Chen, Z. Zhong, J. Chin, H. Mook and Y. F. Han, *Catal. Commun.*, 2007, **8**, 1421.
20 P. Z. Si, D. Li, C. J. Choi, Y. B. Li, D. Y. Geng and Z. D. Zhang, *Solid State Commun.*, 2007, **142**, 723.
21 S. Lei, K. Tang, Z. Fang, Q. Liu and H. Zheng, *Mater. Lett.*, 2006, **60**, 53.
22 Z. W. Chen, J. K. L. Lai and C. H. Shek, *J. Non-Cryst. Solids*, 2006, **352**, 3285.
23 Z. Yang, W. Zhang, Q. Wang, X. Song and Y. Qian, *Chem. Phys. Lett.*, 2006, **418**, 46.
24 K. F. Lin, H. M. Cheng, H. C. Hsu, L. J. Lin and W. F. Hsieh, *Chem. Phys. Lett.*, 2005, **409**, 208.
25 Y. Hu, T. Mei, J. Guo and T. White, *Inorg. Chem.*, 2007, **46**, 11031.
26 Y. Hu, H. S. Qian, T. Mei, J. Guo and T. White, *Mater. Lett.*, 2010, **64**, 1095.
27 L. J. Wang and N. C. Giles, *J. Appl. Phys.*, 2003, **94**, 973.
28 R. R. Chevalier, G. Roult and E. F. Bertaut, *Solid State Commun.*, 1967, **5**, 7.
29 R. W. Grant, S. Geller, J. A. Cape and G. P. Espinosa, *Phys. Rev.*, 1968, **175**, 686.
30 M. Regulski, R. Przenioslo, I. Sosnowska, D. Howhlwein and R. Schneider, *J. Alloys Compd.*, 2004, **362**, 236.
31 F. Jiao, A. Harrison, A. H. Hill and P. G. Bruce, *Adv. Mater.*, 2007, **19**, 4063.

